Journal of Catalysis 262 (2009) 235–243

Contents lists available at ScienceDirect

Journal of Catalysis

www.elsevier.com/locate/jcat

Pd-promoted selective gas phase hydrogenation of *p*-chloronitrobenzene over alumina supported Au

Fernando Cárdenas-Lizana [a], Santiago Gómez-Quero [a], Antoine Hugon [b], Laurent Delannoy [b], Catherine Louis [b], Mark A. Keane [a,*]

[a] *Chemical Engineering, School of Engineering and Physical Sciences, Heriot-Watt University, Edinburgh, EH14 4AS, Scotland*
[b] *Laboratoire de Réactivité de Surface, UMR 7609 CNRS, Université Pierre et Marie Curie-Paris 06, 4 Place Jussieu, 75252 Paris Cedex 05, France*

ARTICLE INFO

Article history:
Received 18 November 2008
Revised 22 December 2008
Accepted 23 December 2008
Available online 22 January 2009

Keywords:
p-Chloronitrobenzene
Selective hydrogenation
p-Chloroaniline
Au/Al_2O_3
$Pd–Au/Al_2O_3$
DRIFTS analysis
TPR
H_2 chemisorption

ABSTRACT

The gas phase hydrogenation of *p*-chloronitrobenzene has been investigated over alumina supported Au (ca. 1%, w/w) prepared by deposition-precipitation with urea (DP) and impregnation in excess solvent (IMP). Both catalysts were 100% selective in terms of $–NO_2$ group reduction, resulting in the sole formation of *p*-chloroaniline. Au–DP exhibited a smaller mean Au size (2.9 nm) compared with Au–IMP (4.5 nm) and delivered a higher (by a factor of 14) specific hydrogenation rate. Bimetallic $Pd–Au/Al_2O_3$ catalysts have also been prepared by DP and IMP with Au/Pd mol/mol = 8, 20 and 88. Catalyst activation by temperature programmed reduction has been monitored and the activated catalysts characterized in terms of H_2 chemisorption, TEM analysis and DRIFTS. DRIFTS measurements using CO as a probe molecule suggest the presence of bimetallic particles and surface Au–Pd interaction. A significant increase (by up to a factor of 3) in activity was observed for $Pd–Au/Al_2O_3$ (Au/Pd $\geqslant$ 20) compared with Au/Al_2O_3 where the exclusive conversion of *p*-chloronitrobenzene to *p*-chloroaniline was maintained. At a lower ratio (Au/Pd = 8), nitrobenzene was produced as a result of a Pd catalyzed hydrodechlorination step. Under the same reaction conditions, $Au/Al_2O_3 + Pd/Al_2O_3$ physical mixtures (Au/Pd = 20) delivered higher reaction rates but with the formation of nitrobenzene and aniline, i.e. products of hydrodechlorination and hydrogenation. We attribute the enhanced and exclusive production of *p*-chloroaniline over the supported bimetallics to a surface Pd–Au synergism. Our results establish the viability of Pd-promotion in the selective continuous gas phase catalytic hydrogenation of *p*-chloronitrobenzene over supported Au.

1. Introduction

Halogenated aromatic amines, with multiple applications in the manufacture of pesticides, herbicides, pigments, pharmaceuticals and cosmetics, are commercially important target products [1]. Existing routes, notably the Bechamp process (Fe promoted reduction in acid media), produce toxic by-products with low overall product yields [2] and there is now a pressing demand for a cleaner technology. We have recently demonstrated that the gas phase hydrogenation of *p*-chloronitrobenzene over Au supported on alumina [3,4] and titania [4] was 100% selective in terms of $–NO_2$ group reduction to *p*-chloroaniline over a prolonged (up to 80 h) time on-stream. However, the level of *p*-chloronitrobenzene conversion was appreciably lower than that delivered by supported Pd, which generated nitrobenzene and aniline (non-selective hydrogenation) as the principal products with a significant temporal loss of activity [3]. Indeed, two possible reaction pathways are associated with the hydrogenation of *p*-chloronitrobenzene [3,5], as shown in Fig. 1. Path A involves hydrodechlorination to nitrobenzene, which can be further hydrogenated to aniline *via* the nitrosobenzene intermediate. In Path B, the $–NO_2$ group is initially hydrogenated to yield the target product (*p*-chloroaniline), which can undergo subsequent hydrodechlorination to aniline. Both mechanisms have been reported for gas and/or liquid phase catalytic operation over supported metals [3,6–13]. Dechlorination at high conversions is a feature of reactions promoted by supported Ni [7,8], Pd [11,14], Pt [12,13,15], Ru [16], bi-metallic La–NiB [9], Pd–Ru [10], Pd–Pt [10], Pt–M (M = Cr, Mn, Fe, Co, Ni and Cu) [17] and Pt–M (M = Sn, Pb, Ge, Al, Zn) [18] catalysts. Xu et al. [19] have reported that the incorporation of Sn^{4+} in Pd/Al_2O_3 served to limit the degree of *p*-chloronitrobenzene dechlorination in batch liquid reaction and attributed this effect to interaction between Sn^{4+} and the $–NO_2$ group that increased the polarity of the N=O bond and promoted reduction. However, higher conversions of *p*-chloronitrobenzene were accompanied by a decrease in selectivity to *p*-chloroaniline. The main goal of our work is to direct the reaction along Path B,

* Corresponding author.
E-mail address: m.a.keane@hw.ac.uk (M.A. Keane).

0021-9517/$ – see front matter
doi:10.1016/j.jcat.2008.12.019

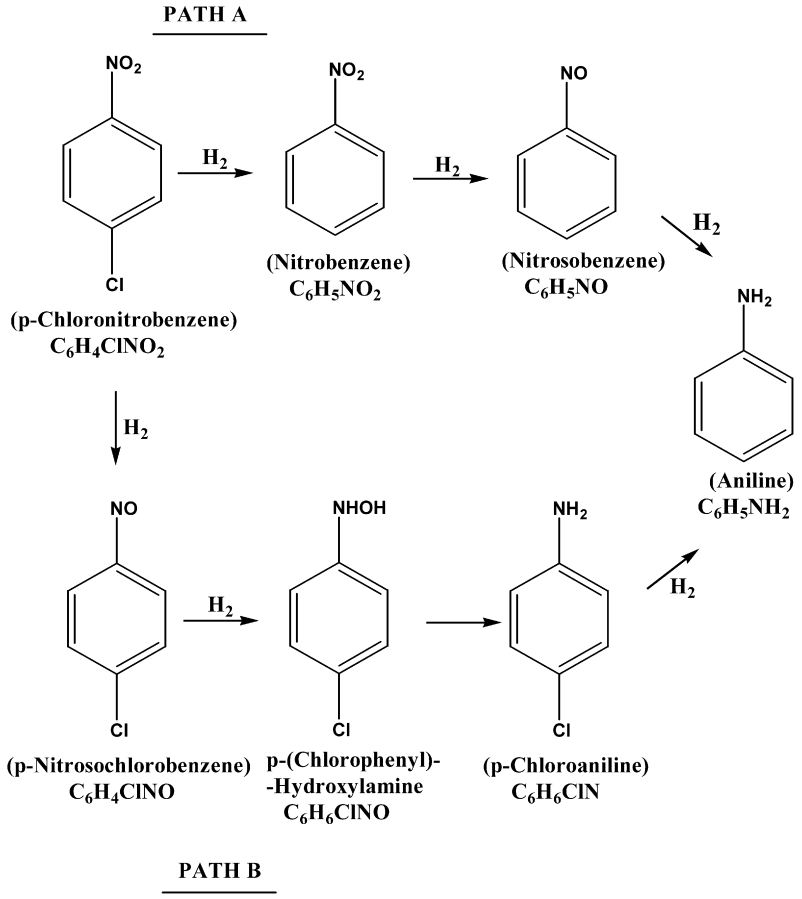

Fig. 1. Reaction pathways associated with the hydrogen mediated conversion of *p*-chloronitrobenzene.

elevating the level of *p*-chloroaniline production without the formation of aniline in continuous flow operation.

Catalytic hydrogenation over supported Au has been proposed to depend on the preparation method [20], metal particle size/morphology [21] and support surface chemistry [22]. The optimum supported Au particle size is still a matter of some debate but it is commonly accepted that, in order to achieve high activity, the presence of particles smaller than ca. 5 nm is crucial. An increase in Au dispersion, with a consequent decrease in Au particle size, increases the proportion of surface low coordination sites on which H_2 can dissociate [23,24]. Nevertheless, there is some evidence of a lower limit in terms of Au particle size (ca. 2 nm), below which activity decreases due to quantum effects [25,26]. The ultimate degree of dispersion is dependent on catalyst synthesis and Okumura et al. [27] obtained, in the case of (ca. 1%, w/w) Au/Al_2O_3 prepared by deposition-precipitation (DP) and impregnation (IMP), an order of magnitude difference in the mean Au diameter (DP = 3 nm, IMP = 37 nm). Grisel et al. [28] also recorded an appreciably smaller Au particle size (3–5 nm) by DP synthesis when compared with IMP. Catalytic activity may also be enhanced through the use of promoters, which can serve to modify the electronic properties of the active site [29]. In the case of Au catalysis, the number of studies that have considered the use of promoters in hydrogenation reactions is very limited but we can flag the work of Gluhoi et al. [30,31] who demonstrated enhanced activity in NO reduction over Al_2O_3-supported combinations of Au with CeO_x and LiO_2, ascribing the promotional effect of the metal oxides to the formation of small and thermally stable Au particles. Moreover, Nutt et al. [32] reported enhanced activity in the hydrogen mediated dechlorination of C_2HCl_3 over $Au–Pd/Al_2O_3$ when compared with Pd/Al_2O_3 which they attributed to Au/Pd interactions, an effect that extended to unsupported Au/Pd nanoparticles [33].

With a view to elevating the catalytic activity of Au, we have considered the possible role of Pd, with high activity in gas phase $–NO_2$ group reduction [3,5,34–36], as a promoter. In this paper, we examine, for the first time, the catalytic action of Pd promoted Au/Al_2O_3 ($Au/Pd \geqslant 8$) in the selective reduction of *p*-chloronitrobenzene to *p*-chloroaniline. We also assess the feasibility of increasing hydrogenation rate, while maintaining exclusivity in terms of $–NO_2$ reduction, by controlling Au particle size during catalyst preparation and compare IMP and DP as two distinct synthesis routes.

2. Experimental

2.1. Catalyst preparation and activation

The monometallic Au and bimetallic Pd–Au catalysts were prepared by deposition-precipitation (DP) with urea [37] and impregnation (IMP) in excess solvent using Al_2O_3 (AluC Degussa, 110 $m^2\,g^{-1}$) as support. In the case of the DP synthesis, a suspension of the support (3 g) in distilled water (100 cm^3) was placed in an ultrasound bath in order to disperse the support particles. The suspension was then placed in a reactor, 190 cm^3 of distilled water was added and the mixture was heated to 353 K at which point 6 cm^3 of a solution of $HAuCl_4$ (10 $g\,dm^{-3}$), corresponding to the desired Au loading (1%, w/w), was added with a ca. 100-fold excess of urea. The pH of the suspension (initially ca. 2.5) progressively increased to reach ca. 7 after 16 h. The solids obtained were separated by centrifugation, washed three times with deionized water (with centrifugation between each washing) and dried

Table 1
Metal content, residual Cl content, T_{max} and associated H_2 consumption during TPR, H_2 chemisorption values, metal particle size (d_p) and BET surface areas for the mono- and bimetallic catalysts prepared by deposition/precipitation (DP) and impregnation (IMP).

Catalyst	Au (%, w/w)	Au/Pd	Cl content (ppm)	TPR T_{max} (K)	TPR H_2 consumption ($\mu mol\, g^{-1}_{catalyst}$)	H_2 uptake ($\mu mol\, g^{-1}_{Au}$)	d_p (nm)	BET area ($m^2\, g^{-1}_{catalyst}$)
Au–DP	0.88	–	<200	450	62	33	2.9	112
Pd/Au–DP	0.87	88	<200	453	62	47	1.9[a]	97
Pd/Au–DP	0.87	20	300	454 (434)[b]	68	84 (62)[b]	2.0[a]	100 (98)[b]
Pd/Au–DP	0.95	8	1381	491	75	109	2.7[a]	98
Au–IMP	0.81	–	9800	494	62	38	4.5	104
Pd/Au–IMP	0.87	20	14,300	471 (444)[c]	68	30 (23)[c]	5.3[a]	92 (95)[c]

[a] Refers to total metal (Au and Pd) mean particle size.
[b] Results for the physical mixture of Pd–DP + Au–DP (see Section 2).
[c] Results for the physical mixture of Pd–IMP + Au–IMP (see Section 2).

under vacuum at 298 K for 12 h. For the bimetallic catalysts, an adequate volume of a solution of $PdCl_2$ (1 g dm^{-3}) was added to the gold solution to give nominal atomic Au/Pd ratios = 5, 10 and 20. Because of the formation of soluble Pd^{2+} amino species during DP with urea, the experimentally determined (see Table 1) metal loadings corresponded to Au/Pd ratios = 8, 20 and 88, respectively.

In the synthesis by IMP, Al_2O_3 (3 g) was dispersed in 25 cm^3 distilled water in a round bottomed flask (100 cm^3), appropriate volumes of $HAuCl_4$ (10 g dm^{-3}) and (in the case of the bimetallic) $PdCl_2$ (1 g dm^{-3}) were added to achieve a Au/Pd ratio equal to 20 and the resulting slurry was vigorously stirred for 10 min. Excess water was removed on a rotary evaporator at 353 K over 1 h and then dried under vacuum at 298 K for 12 h. Two reference monometallic Pd/Al_2O_3 samples were also prepared by DP (320 ppm Pd, <200 ppm Cl) and IMP (297 ppm Pd, 630 ppm Cl), i.e. with a Pd loading corresponding to that in the Pd–Au samples where Au/Pd = 20. In the case of Pd–IMP, 3 g Al_2O_3 were dispersed in 29 cm^3 distilled water, 1.25 cm^3 $PdCl_2$ (1 g dm^{-3}) solution were added and the resulting slurry was stirred vigorously for 1 h. Excess water was removed on a rotary evaporator at 353 K over a 1 h period and the sample was dried at 393 K for 12 h. In the preparation of Pd–DP, 3 g Al_2O_3 were dispersed in 150 cm^3 distilled water at room temperature to which 1.25 cm^3 of a $PdCl_2$ (1 g dm^{-3}) solution was added with continuous stirring. Because of the formation of soluble Pd^{2+} species when urea is used, Na_2CO_3 was employed as the precipitating agent. The pH was increased by the dropwise addition of a Na_2CO_3 (1 M) solution until it reached 10.5 and the suspension was stirred for 1 h at room temperature; the solid was recovered, washed and dried as above.

After preparation, the samples were stored at 298 K under vacuum (in the dark) in a desiccator. The metal loading was determined (to within ±2%) by inductively coupled plasma-optical emission spectrometry (ICP-OES, Vista-PRO, Varian Inc.) from the diluted extract of aqua regia. The Cl content was measured by silver potentiometric titration after combustion in a Schöniger flask. Prior to use in catalysis, the samples (sieved into a batch of 75 μm average diameter) were activated in 60 $cm^3\, min^{-1}$ H_2 at 3 K min^{-1} to 573 K (Au/Al_2O_3) or 773 K (Pd/Al_2O_3 and $Pd–Au/Al_2O_3$), which was maintained for 2.5 h. After activation, the samples were passivated in 1% (v/v) O_2/He at room temperature for off-line analysis. Physical mixtures of reduced/passivated Pd–DP + Au–DP and Pd–IMP + Au–IMP (Au/Pd atomic ratio = 20) were also examined.

2.2. Catalyst characterization

BET surface area, temperature programmed reduction (TPR) and H_2 chemisorption were determined using the commercial CHEMBET 3000 (Quantachrome) unit. The samples were loaded into a U-shaped Pyrex glass cell (10 cm × 3.76 mm i.d.) and heated in 17 $cm^3\, min^{-1}$ (Brooks mass flow controlled) 5% (v/v) H_2/N_2 to 573 K (Au/Al_2O_3) or 773 K (Pd/Al_2O_3 and $Pd–Au/Al_2O_3$) at 3 K min^{-1}. The effluent gas passed through a liquid N_2 trap and changes in H_2 consumption were monitored by TCD with data acquisition/manipulation using the TPR Win™ software. The reduced samples were maintained at the final temperature for 2.5 h in a constant flow of H_2, swept with 65 $cm^3\, min^{-1}$ N_2 for 1.5 h, cooled to room temperature and subjected to H_2 chemisorption using a pulse (10 μl) titration procedure. BET areas were recorded with a 30% (v/v) N_2/He flow using pure N_2 (99.9%) as internal standard. At least 2 cycles of N_2 adsorption–desorption in the flow mode were employed to determine total surface area using the standard single point method. BET surface areas and H_2 uptake values were reproducible to within ±5%; the values quoted represent the mean. TEM analysis was performed using a JEOL 100 CX II microscope where the average metal particle sizes were established from a measurement of at least 300 particles. The size limit for the detection of gold particles on Al_2O_3 is ca. 1 nm. Infrared spectroscopy was performed with an IFS 66V Bruker spectrometer using a DRIFTS cell. The catalyst precursors (10–20 mg) were reduced *in situ* by TPR (conditions as described above). The cell was then purged with He at 298 K before introducing a flow (50 $cm^3\, min^{-1}$) of 1% (v/v) CO in He. The spectrum recorded under He was used as reference and the intensity of the spectrum under CO/He is expressed as $\log(I_{CO}/I_{ref})$.

2.3. Catalysis procedure

Reactions were carried out under atmospheric pressure at T = 393 K, *in situ* immediately after activation, in a continuous fixed bed vertical glass reactor (l = 600 mm; *i.d.* = 15 mm). The catalytic reactor and operating conditions to ensure negligible heat/mass transport limitations, have been fully described elsewhere [38] but some features, pertinent to this study, are given below. A layer of borosilicate glass beads served as a preheating zone, ensuring that the *p*-chloronitrobenzene was vaporized and reached reaction temperature before contacting the catalyst. Isothermal conditions (±1 K) were ensured by diluting the catalyst bed with ground glass (75 μm); the ground glass was mixed thoroughly with catalyst before insertion into the reactor. Reaction temperature was continuously monitored by a thermocouple inserted in a thermowell within the catalyst bed. The reactant was delivered to the reactor *via* a glass/Teflon airtight syringe and Teflon line using a microprocessor controlled infusion pump (Model 100 kd Scientific) at a fixed calibrated flow rate. A co-current flow of *p*-chloronitrobenzene and ultra pure H_2 (<1% v/v *p*-chloronitrobenzene/H_2) was maintained at a GHSV = 2×10^4 h^{-1} with an inlet *p*-chloronitrobenzene molar flow (F) over the range 0.1–0.4 mmol h^{-1}, where the H_2 content was up to 200 times in excess of the stoichiometric requirement (P_{H_2} = 0.92 atm), the flow rate of which was monitored using a Humonics (Model 520) digital flowmeter. The molar metal (n) to inlet *p*-chloronitrobenzene feed rate ratio spanned the range

1×10^{-3}–14×10^{-3} h. In a series of blank tests, passage of *p*-chloronitrobenzene in a stream of H_2 through the empty reactor or over the support alone, i.e. in the absence of Pd, Au or Pd–Au, did not result in any detectable conversion. The reactor effluent was frozen in a liquid nitrogen trap for subsequent analysis, which was made using a Perkin–Elmer Auto System XL gas chromatograph equipped with a programmed split/splitless injector and a flame ionization detector, employing a DB-1 50 m × 0.20 mm i.d., 0.33 μm film thickness capillary column (J&W Scientific), as described elsewhere [39]. A chlorine (in the form of HCl) mass balance was performed by passing the effluent gas through an aqueous NaOH trap (7.0×10^{-4} mol dm^{-3}, kept under constant agitation at 400 rpm) with independent pH (Hanna HI Programmable Printing pH Bench-Meter) analysis. Repeated (up to five separate) catalytic runs with different samples from the same batch of catalyst delivered product compositions that were reproducible to within ±8%. *p*-Chloronitrobenzene (Aldrich, ⩾99.9%, w/w, purity) and the 1-butanol solvent (Riedel-de Häen, ⩾99.5%) were used as supplied without further purification.

3. Result and discussion

3.1. Catalyst characterization

3.1.1. TPR, H_2 chemisorption and TEM analysis

The BET surface areas of the activated catalysts (see Table 1) were close to that of the Al_2O_3 support (110 m^2 g^{-1}). The TPR activation profiles for Au/Al_2O_3 prepared by DP (Profile I) and IMP (Profile V) are presented in Fig. 2; the temperatures associated with maximum H_2 consumption (T_{max}) are given in Table 1. Hydrogen consumption during TPR matched (to within ±8%) that required for the reduction of the supported Au precursors. The reduction profile for Au–DP is characterized by a single positive peak at 450 K, which is consistent with the TPR results for Au/Al_2O_3 prepared by DP that have been reported in the literature [40–43]. The occurrence of a single TPR peak has been attributed to Au^{3+} reduction to Au^0 [42,44]. TPR of our Au–IMP sample generated a single T_{max} at 494 K, which is in good agreement with the work of Baatz and Prüße [41] and Gluhoi et al. [43]. Bus and co-workers [45], in their analysis of Au/Al_2O_3 prepared by IMP using time-resolved *in situ* XAS, established the presence of Al_2O_3-supported oxidic or hydroxidic Au^{3+} species in the precursor that were reduced to Au^0 in H_2 at 440 K. The higher reduction temperature recorded for Au–IMP compared with Au–DP may be related to the greater residual Cl (see Table 1) associated with the former, which can affect the reducibility of Au(III) [45–49]. Moreover, the mobility of the Cl containing precursor after impregnation is known to induce Au sintering during activation [50–52]. This can account for the larger mean Au particle size in the Au–IMP sample (see Table 1). Representative TEM images are included in Fig. 3, which serve to illustrate the nature of the metal dispersion in these catalysts. It can be seen that the Au component is present as discrete particles with a quasi-spherical morphology.

Taking the Pd/Au–DP samples (see Fig. 2, Profiles II, III and IV), a progressive shift of the reduction peak to higher temperatures was observed with increasing Pd content. In previous studies [3,5], we have recorded a negative peak (H_2 release at 340–380 K) during the TPR of Pd/Al_2O_3 that we attributed to the decomposition of β-Pd hydride formed by the absorption of H_2 on zero valent Pd when the H_2 pressure exceeds 0.02 atm [53]. In the case of our Pd/Au samples, there was no detectable H_2 release but this can be due to the low Pd content. In addition to H_2 release/hydride decomposition, Pd/Al_2O_3 has been reported to exhibit H_2 consumption where $T > 573$ K due to the reduction of oxidized Pd species that interact strongly with the support [54]. The broad peaks observed for Pd/Au–DP (453–491 K) may be the result of a composite

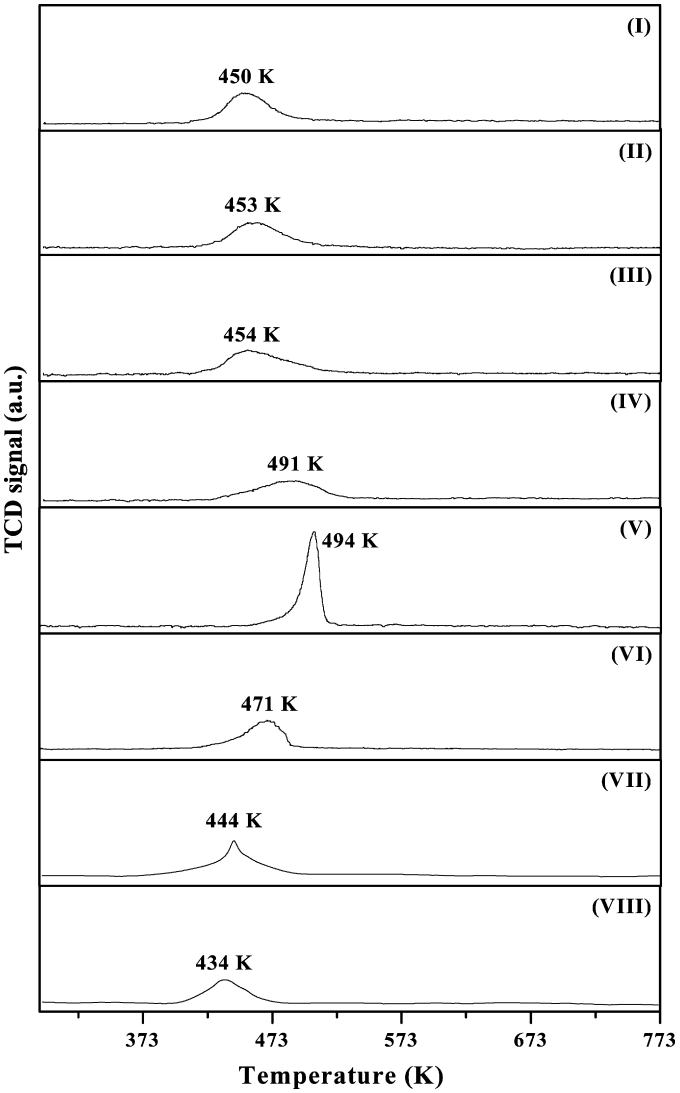

Fig. 2. TPR profiles for: (I) Au–DP; (II) Pd/Au–DP (Au/Pd = 88); (III) Pd/Au–DP (Au/Pd = 20); (IV) Pd/Au–DP (Au/Pd = 8); (V) Au–IMP; (VI) Pd/Au–IMP (Au/Pd = 20); (VII) Au–IMP + Pd–IMP (Au/Pd = 20); (VIII) Au–DP + Pd–DP (Au/Pd = 20).

reduction of both metals, suggesting some interaction between Au and Pd species that modifies their respective reducibility. Hosseini et al. [55], using co-deposited $Au–Pd/TiO_2$ noted a shift in the reduction peak for PdO (with the introduction of Au) from 433 (100 Pd at%) to 373 K (33 Pd at%). In the TPR of Pd/Au–IMP (Profile VI), the reduction peak appears at a lower temperature than that recorded for Au–IMP. This response is the direct opposite of that observed for the DP systems, possibly suggesting a different degree of interaction between Au and Pd in the IMP sample, which may be affected by the Cl content. The TPR profiles generated for both physical mixtures (Profiles VII and VIII) exhibit a similar response in that the onset of H_2 consumption during reduction was shifted to lower temperatures (with a lower T_{max}, see Table 1) than that observed for the Au/Al_2O_3 systems. The inclusion of Pd/Al_2O_3 in the mixture must serve to facilitate the reduction of Au/Al_2O_3, possibly through the involvement of spillover hydrogen generated by the Pd component.

Hydrogen uptake (see Table 1) on both Au/Al_2O_3 samples was low, which is consistent with reports [56,57] that have demonstrated a limited capacity of Au to chemisorb hydrogen. This can be linked to the high activation energy barrier required for the dissociative adsorption of hydrogen on Au [45,58]. The incorpo-

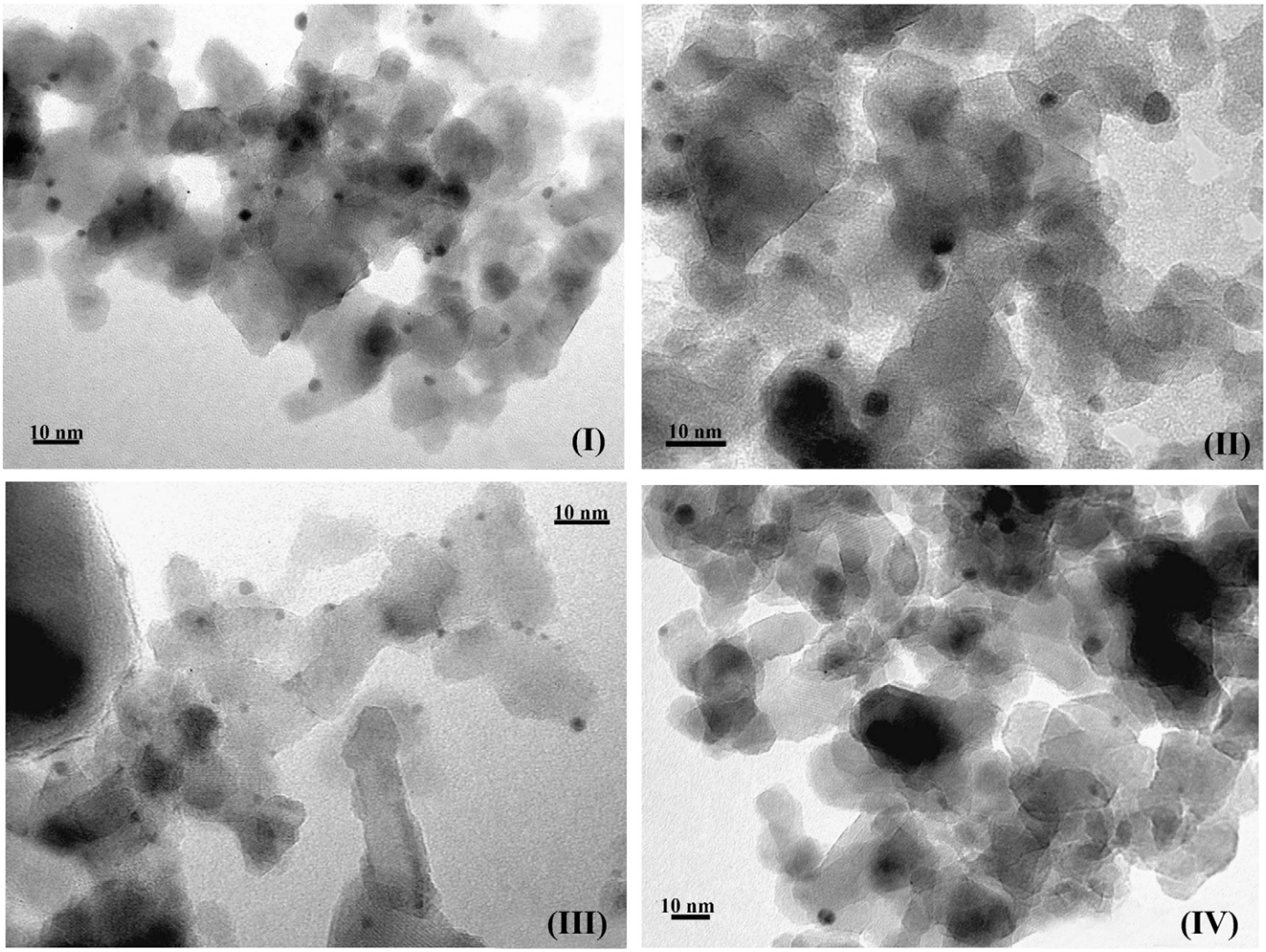

Fig. 3. Representative TEM images of (I) Au–DP, (II) Au–IMP, (III) Pd/Au–DP (Au/Pd = 20) and (IV) Pd/Au–IMP (Au/Pd = 20).

ration (chemically or as a physical mixture) of Pd resulted in an increase in H_2 uptake. In the case of the DP samples (see Table 1), it was proportional to the Pd content. The higher uptake on Pd/Au–DP (Au/Pd = 20) compared with the corresponding physical mixture suggests a surface Pd–Au synergy that serves to increase the chemisorption capacity. In the case of the IMP system, the inclusion of Pd did not result in an increase in H_2 uptake. This response may be due to the higher Cl content that acts to suppress H_2 chemisorption allied to the larger particle size observed by TEM (see Table 1). Indeed, it has been shown [47,59] that Cl and Br can act to inhibit CO uptake on Au where CO also adsorbs on low coordination surface sites. The monometallic Pd reference catalysts (DP or IMP) did not generate any signal during TPR and did not exhibit any measurable H_2 chemisorption, which we attribute to the very low Pd content resulting in experimental measurements that fell below instrumental detector limits.

3.1.2. DRIFTS analysis

DRIFTS analysis using CO as a probe molecule was performed and the resultant spectra are given in Fig. 4. The spectra of the carbonyl region for Pd–DP (Profile I) and Pd–IMP (Profile II) are similar and can be divided into two regions, i.e. high (2200–2000 cm^{-1}) and low (2000–1800 cm^{-1}) wave numbers. The bands at high wave numbers have been assigned in the literature [60] to linearly adsorbed carbonyl species on different Pd crystal planes (2105–2070 cm^{-1}). Those at low wave numbers have been related to bridged (two-fold bound, 2000–1895 cm^{-1}) and three-fold bound carbonyl species (1920–1830 cm^{-1}) on metallic Pd [60,61]. The Au–DP sample (Profile III) shows an intense single band at 2105 cm^{-1}, which has been previously associated with CO linearly adsorbed on low coordination sites of metallic Au nanoparticles [62–64]. The spectrum of Au–IMP (Profile IV) is characterized by a broad band with a maximum at 2063 cm^{-1} and a weak broad band at 2127 cm^{-1}. The presence of bands at wave numbers lower than those for CO linearly adsorbed on metallic Au (around 2100 cm^{-1}) has been reported previously [65–69]. The formation of bridged CO species can be discounted as they give rise to bands around 2000–1950 cm^{-1} [65,66]. Bands observed in the region 2050–2080 cm^{-1} can be ascribed either to CO adsorbed on metallic sites at the support/particle interface [67,68] or to CO adsorbed on negatively charged $Au^{\delta-}$ sites [65,68]. The presence of $Au^{\delta-}$ in Au–IMP can result as a consequence of the high chloride content (Table 1). The residual chloride may be located either on the alumina support in close proximity to the Au particles or associated directly with the Au particles as reported in recent papers [47,70,71]. Computer modeling of Cl^- interactions with Au (111) has revealed that Cl^- adsorption on Au^0 should result in a 0.05 positive electric charge associated with the Cl atom while the conjoined Au atom should develop a 0.190 negative electric charge where the other surface Au atoms adopt a negative charge from 0.05 to 0.08 [72]. The weak band at 2127 cm^{-1} has been previously assigned either to CO adsorbed on metallic Au at low CO

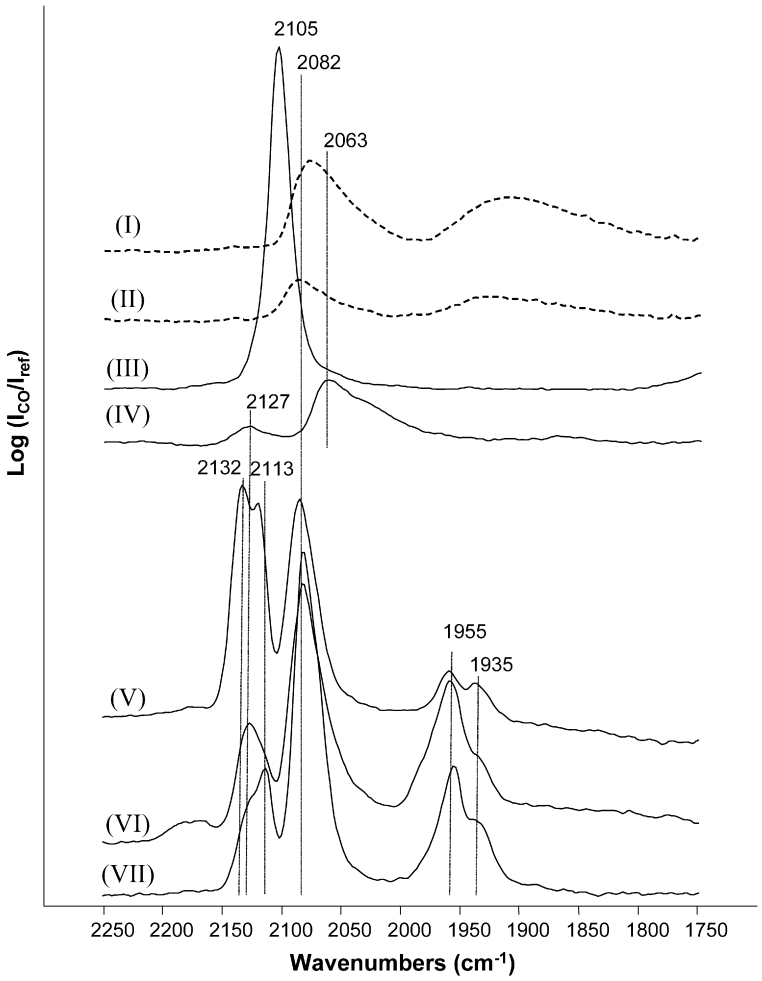

Fig. 4. DRIFTS spectra (under 1%, v/v, CO/He at 298 K) of (I) Pd–DP, (II) Pd–IMP, (III) Au–DP, (IV) Au–IMP, (V) Pd/Au–IMP (Au/Pd = 20), (VI) Pd/Au–DP (Au/Pd = 8) and (VII) Pd/Au–DP (Au/Pd = 20).

coverage [20,60,73] or to CO-$Au^{\delta+}$ species [74–77]. At this juncture, we cannot propose a definitive interpretation for this band but it is important to note that the IR spectra of Au–IMP and Au–DP are quite distinct. We associate these differences with the higher chloride content and the slightly larger Au particle size exhibited by Au–IMP.

In the case of the three spectra (Profiles V–VII) for the bimetallic catalysts, we also observed carbonyl bands at high (2150–2050 cm^{-1}) and low (2000–1900 cm^{-1}) wave numbers but the spectra deviate significantly from that expected on the basis of the sum of the monometallic Au and Pd contributions (combination of Profiles I and III and Profiles II and IV). The bands at low wave numbers can again be assigned to CO bridged species on Pd crystal planes. However, the broad and poorly resolved feature that characterized the monometallic Pd samples (Profiles I and II) is transformed into two resolved peaks at 1955 and 1935 cm^{-1} for the bimetallic Pd–Au catalysts, i.e. at a higher wave number than that which characterizes three-fold bound carbonyl species on Pd. These observations suggest the absence of three-fold CO bridges and the presence of only two-fold bridged species. At higher frequencies, a band at ~2082 cm^{-1} is observed for all the Pd–Au catalysts at a similar frequency to that of linear adsorbed CO on Pd but with a greater intensity. It should be noted that the band at 2105 cm^{-1}, associated with CO linearly adsorbed on gold, exhibits an appreciable decrease in intensity. By analogy with observations reported for Au–Pd films [78] and Au–Pd clusters on silica films [79], the disappearance of the three-fold bridge band and concomitant increases in intensity of the band due to linear CO on Pd^0 (with the decrease in intensity of the band due to linear CO on Au^0) represent evidence for the formation of bimetallic particles. The dilution of Pd in Au limits the extent of multi-bonded CO on Pd, especially three-fold bridge CO formation and thus favors linear interaction between CO and any isolated Pd^0 sites. The spectra of our Au–Pd samples also show bands at higher wave numbers (2110–2135 cm^{-1}), which were not systematically observed on Au–Pd films [78,80] or Au–Pd clusters [79]. However, in the latter case, a frequency shift of the band for CO linearly adsorbed on Au clusters (from 2109 to 2129 cm^{-1}) was noted with a decrease in CO coverage. Accordingly, we tentatively assign the bands at 2110–2135 cm^{-1} to CO linearly adsorbed on Au^0 sites in monometallic or bimetallic particles. Our DRIFTS results indicate that, in the case of the Pd–Au samples, the contribution of multi-bonded CO on Pd is reduced with respect to the linearly bonded CO on Pd. A geometric effect, due to the formation of bimetallic Pd–Au nanoparticles and resulting in a decrease in the size and/or the number of Pd ensembles required for multiple bonding (three-fold), can account for this response [78,79,81]. This suggests that there is a larger proportion of isolated singleton Pd sites in the Pd–Au/Al_2O_3 catalysts prepared by both DP and IMP. It should be noted that the slight shift of the band due to CO linearly adsorbed on Pd^0 in the Au–Pd samples has also been also observed by Goodman et al. [78] and attributed to changes in dipole–dipole coupling due to variations in CO intermolecular distances rather than to chemical interaction mediated by the substrate, i.e. an electronic effect.

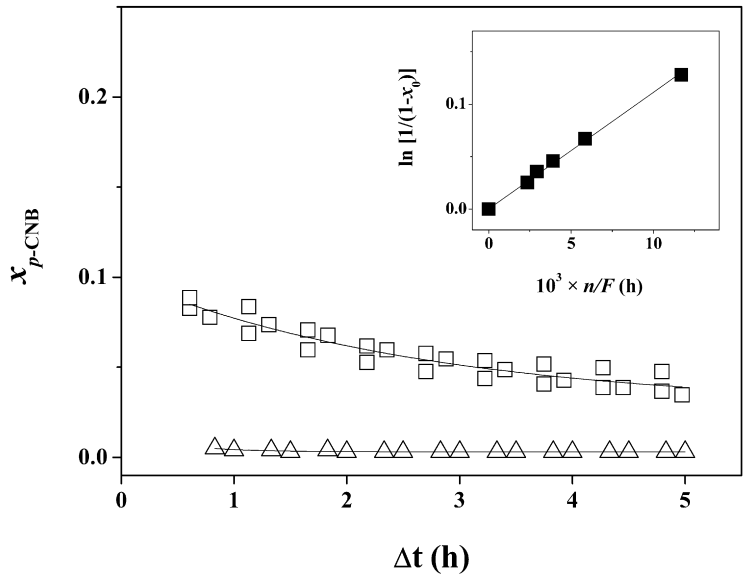

Fig. 5. Variation of *p*-chloronitrobenzene fractional conversion ($x_{p\text{-CNB}}$) with time-on-stream over (△) Au–IMP (*p*-chloronitrobenzene/Au = 74 $mol_{p\text{-CNB}}\,mol_{Au}^{-1}\,h^{-1}$) and (□) Au–DP (*p*-chloronitrobenzene/Au = 284 $mol_{p\text{-CNB}}\,mol_{Au}^{-1}\,h^{-1}$). Inset: Pseudo-first order kinetic plot for the hydrogenation of *p*-chloronitrobenzene over Au–DP.

3.2. Catalytic response

Hydrogenation of *p*-chloronitrobenzene over Au–DP and Au–IMP generated exclusively the target product, *p*-chloroaniline, with no evidence of any hydrodenitrogenation, hydrodechlorination or ring reduction, in agreement with our earlier work [3,4]. The time-on-stream profiles for the conversion of *p*-chloronitrobenzene over both Au/Al_2O_3 catalysts are shown in Fig. 5 where it can be seen that Au–DP delivered a consistently higher fractional conversion ($x_{p\text{-CNB}}$) than Au–IMP. The temporal variation of activity can be represented by [82]

$$\frac{(x_{p\text{-CNB}} - x_0)}{(x_{5\ h} - x_0)} = \frac{\Delta t}{(\beta + \Delta t)},$$

where $x_{5\ h}$ represents fractional conversion after 5 h on-stream and β is a time scale fitting parameter. Fit convergence yields values for x_0, the initial fractional conversion, which is a measure of initial activity. The applicability of pseudo-first order kinetics can be tested using the following kinetic expression

$$\ln(1 - x_0)^{-1} = k\left(\frac{n}{F}\right)$$

and is demonstrated in the inset to Fig. 5 for Au–DP. The extracted pseudo-first order rate constants are given in Table 2. Converting the raw (experimental) rate constants to specific rates (per Au surface area, based on the mean Au particle size obtained from TEM), Au–DP delivered a rate (418 $\mu mol\,m_{Au}^{-2}\,h^{-1}$) that was over an order of magnitude higher than that recorded for Au–IMP (29 $\mu mol\,m_{Au}^{-2}\,h^{-1}$). This suggests that smaller Au particles are intrinsically more active. Taking an overview of the available literature, the role of Au particle size in hydrogenation reactions appears to be dependent on the nature of the reaction [83], the support [84] and even the catalyst preparation method [85]. Although under optimum reaction conditions, Au particles as large as 20 nm can exhibit significant activity [86], the general trend suggests increasing hydrogenation efficiency over smaller Au particles ($\leqslant$10 nm) [56]. Mohr et al. [21] have considered the hydrogenation of acrolein to allyl alcohol over Au/TiO_2 and Au/ZrO_2 catalysts which exhibited similar Au particle sizes. The Au/TiO_2 catalyst was approximately twice as active and more selective in terms of allyl alcohol production, a response that was attributed to a greater preponderance of uncoordinated Au atoms associated with the titania support. Jia et al. [87] have recorded a maximum acetylene hydrogenation over Au/Al_2O_3 bearing Au particles of 3 nm diameter while Zanella et al. [24] have reported a significant increase in crotonaldehyde hydrogenation turnover frequency (TOF) over Au/TiO_2 with a decrease in Au particle size from 8.7 to 1.7 nm. The higher TOF exhibited by smaller Au particles may be associated with an increased capacity to activate/dissociate hydrogen [23,24]. Stobiński et al. [88] proposed that the chemisorption of H_2 is facilitated on Au surface atoms with low coordination number to form a AuH_2 complex. The lower activity associated with Au–IMP may also be related to the higher residual Cl content (Table 1). Indeed, we have demonstrated elsewhere [46] that the presence of chloride in Au/Al_2O_3 samples served to lower butadiene hydrogenation activity regardless of Au particle size. DRIFTS analysis has indicated that the presence of surface Cl species can induce strong modifications to the electronic state of the Au particles, which may affect reactant adsorption/activation and impact on hydrogenation performance. Indeed, there is evidence in the literature [47,49,70,72] that halides can adsorb on metallic gold with a resultant suppression of reactant adsorption. In short, the observed catalytic response for the monometallic samples where Au–DP outperformed Au–IMP can be attributed to a composite effect due to higher intrinsic activity for smaller Au particles (Au–DP) and the deleterious effects of surface Cl (Au–IMP).

Table 2
Pseudo-first order initial rate constants (k) for the hydrogenation of *p*-chloronitrobenzene over mono- and bimetallic catalysts and monometallic physical mixtures with product selectivities at the same initial fractional conversion ($x_0 \sim 0.12$).

Catalyst	Au/Pd	Rate constant (k, h^{-1})	Product(s) (% selectivity)
Au–DP	–	12	*p*-Chloroaniline (100)
Pd/Au–DP	88	24	*p*-Chloroaniline (100)
Pd/Au–DP	20	39	*p*-Chloroaniline (100)
Pd/Au–DP	8	92	*p*-Chloroaniline (80) Nitrobenzene (20)
Au–IMP	–	1	*p*-Chloroaniline (100)
Pd/Au–IMP	20	22	*p*-Chloroaniline (100)
Pd–IMP + Au–IMP	20	130	Nitrobenzene (80) Aniline (20)
Pd–DP + Au–DP	20	77	Nitrobenzene (45) Aniline (55)

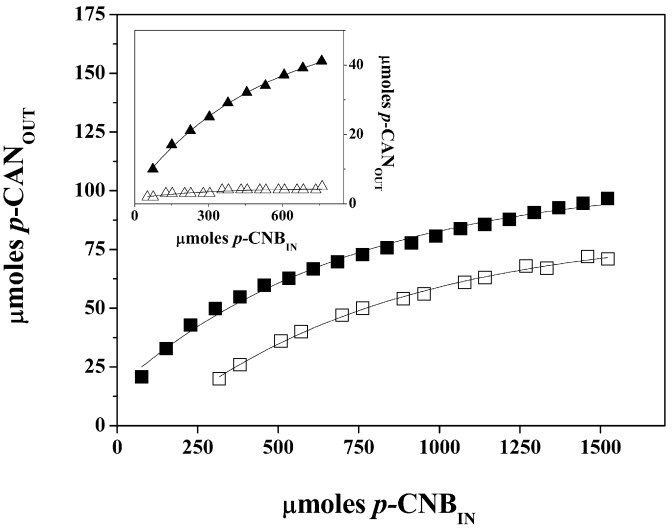

Fig. 6. *p*-Chloroaniline output (μmoles *p*-CAN_{OUT}) as a function of the number of moles of *p*-chloronitrobenzene that had been processed (μmoles *p*-CNB_{IN}) over Au–DP (□) and Pd/Au–DP (■, Au/Pd = 20). Inset: Au–IMP (△) and Pd/Au–IMP (▲, Au/Pd = 20); inlet Au/*p*-chloronitrobenzene = 1×10^{-2} $mol_{metal}\,h\,mol^{-1}_{p\text{-}CNB}$.

In earlier work [3], we reported that the incorporation of Au with Pd *via* reductive deposition to generate Au–Pd/Al_2O_3 (where Pd/Au = 10) did not influence *p*-chloronitrobenzene hydrogenation activity or selectivity, which were equivalent to that delivered by Pd/Al_2O_3, where aniline was the predominant product. In this study, the inclusion of a low Pd content to Au/Al_2O_3 by DP and IMP (Au/Pd > 8) was considered and the results are presented in Fig. 6 and Table 2. The presence of Pd served to significantly raise the hydrogenation rate constant, which increased with increasing Pd content (Table 2). Where Au/Pd ⩾ 20, the reaction was 100% selective in terms of *p*-chloroaniline production with no detectable by-products. At a lower Au/Pd ratio, reaction over Pd–Au/Al_2O_3–DP (Au/Pd = 8) generated *p*-chloroaniline and nitrobenzene, the latter resulting from a hydrodechlorination step (see Fig. 1), which is a characteristic of catalysis by Pd. The combination of both Au/Al_2O_3 and Pd/Al_2O_3 (DP and IMP samples) as physical mixtures (Au/Pd = 20) resulted in the formation of nitrobenzene and aniline (composite hydrodechlorination/hydrogenation product). Such a response demonstrates that, under these reaction conditions, Au/Al_2O_3 had little effect on reaction selectivity, which was governed by the Pd/Al_2O_3 component. This result is consistent with catalytic action due to segregated Pd and Au particles where the catalytic properties of Pd dominate. At Au/Pd = 20, the rate constants delivered by the physical mixtures were appreciably higher than that delivered by Pd–Au/Al_2O_3 (both DP and IMP). Allied to the quite distinct product composition (at an equivalent *p*-chloronitrobenzene conversion, see Table 2), these results demonstrate that the contribution of Pd and Au to the catalytic action of Pd–Au/Al_2O_3 is not merely an additive effect and is the result of a surface Pd/Au synergism. The *p*-chloroaniline produced (μmoles *p*-CAN_{OUT}) as a function of the number of moles of *p*-chloronitrobenzene that had been processed (μmoles *p*-CNB_{IN}) is illustrated in Fig. 6 where it can be seen that the inclusion of Pd ensured an appreciably higher output of the target product for both DP and IMP bimetallics. These results establish the viability of Pd promoted selective $-NO_2$ reduction over supported Au.

3.3. General discussion

The catalytic results demonstrate the bimetallic character of active sites in the Au/Pd–DP and Au/Pd–IMP samples (which promote exclusive formation of *p*-chloroaniline) as opposed to the segregation of both metals in the physical mixtures (leading to the formation of nitrobenzene and aniline). There is, however, an upper limit to the amount of Pd that can be incorporated in the Au system (Au/Pd ⩽ 8), above which the selectivity of Au is diminished by the catalytic action of Pd, resulting in hydrodechlorination with the formation of nitrobenzene. The presence of bimetallic Au–Pd particles is consistent with our TPR and DRIFTS measurements. A feature of the IMP synthesis has been the incorporation of a significant residual Cl content which impacts on the reducibility of gold and induces metal particle sintering with an overall decrease in hydrogenation activity. Our results demonstrate that Pd–Au synthesis by DP with urea is an effective route for the production of efficient supported bimetallic particles. More detailed characterization at the scale of individual metal nanoparticles is, however, necessary to explicitly establish the bimetallic character of the supported particles. Advanced electron microscopy techniques, such as high angle annular dark field (HAADF) or energy filtered transmission electron microscopy (EFTEM) could provide this level of analysis. This is far from straightforward as the low proportion of Pd present renders detection very difficult. Nevertheless, the results presented here demonstrate that the use of Pd as a promoter in Au systems prepared by either co-deposition-precipitation and/or co-impregnation results in the formation of bimetallic Au–Pd particles that promote the exclusive hydrogenation of *p*-chloronitrobenzene to *p*-chloroaniline. The promotional effect of Pd has resulted in a significant increase in hydrogenation rate while still retaining the selectivity due to Au. Future work will examine the applicability of these bimetallic Au–Pd systems to other industrially relevant substituted aromatic hydrogenation processes with a consideration of alternative promoters.

4. Conclusions

The catalytic results presented in this study establish Pd promotion of selective hydrogenation over supported Au, which can be exploited as a cleaner sustainable route for the production of *p*-chloroaniline. Both Au–DP and Au–IMP catalyze the exclusive hydrogenation of *p*-chloronitrobenzene to *p*-chloroaniline where Au–DP delivered a (greater than) order of magnitude higher specific hydrogenation rate, which we can link to smaller Au particle size and a lesser residual Cl content. The inclusion of Pd (at Au/Pd ⩾ 20, IMP and DP) resulted in increased activity while retaining exclusivity to *p*-chloroaniline. At higher Pd contents, a further increase in reaction rate was accompanied by the formation of nitrobenzene as a result of a Pd promoted hydrodechlorination. DRIFTS analysis using CO as a probe molecule has demonstrated a decrease in the contribution due to multi-bonded CO on Pd relative to linearly bonded CO in the bimetallic samples, an effect that we take to be diagnostic of Pd–Au surface interaction.

Acknowledgments

The authors are grateful to Maria-Luz Pérez-Cuevas and Noémie Perret for their contribution to the work and financial support from EPSRC through Grant 0231 110525. CNRS and financial support from the World Gold Council are also acknowledged.

References

[1] A. Boehnecke, J. Kielhorn, G. Konnecker, C. Pohlenz-Michel, I. Mangelsdorf, CICADS Report 48, W.H.O., Geneva, 2003, p. 78.
[2] X.D. Wang, M.H. Liang, J.L. Zhang, Y. Wang, Curr. Org. Chem. 11 (2007) 299.
[3] F. Cárdenas-Lizana, S. Gómez-Quero, M.A. Keane, Catal. Commun. 9 (2008) 475.
[4] F. Cárdenas-Lizana, S. Gómez-Quero, M.A. Keane, ChemSusChem 1 (2008) 215.
[5] F. Cárdenas-Lizana, S. Gómez-Quero, M.A. Keane, Appl. Catal. A 334 (2008) 199.
[6] C. Xi, H. Cheng, J. Hao, S. Cai, F. Zhao, J. Mol. Catal. A Chem. 282 (2008) 80.
[7] Y.-Z. Chen, Y.-C. Chen, Appl. Catal. A 115 (1994) 45.
[8] Y.-C. Liu, C.-Y. Huang, Y.-W. Chen, Ind. Eng. Chem. Res. 45 (2006) 62.

[9] Y.-C. Liu, Y.-W. Chen, Ind. Eng. Chem. Res. 45 (2006) 2973.
[10] Z. Yu, S. Liao, Y. Xu, B. Yang, D. Yu, J. Mol. Catal. A Chem. 120 (1997) 247.
[11] V. Kratky, M. Kralik, M. Mecarova, M. Stolcova, L. Zalibera, M. Hronec, Appl. Catal. A 235 (2002) 225.
[12] B. Coq, A. Tijani, F. Figuéras, J. Mol. Catal. 68 (1991) 331.
[13] V.L. Khilnani, S.B. Chandalia, Org. Proc. Res. Dev. 5 (2001) 257.
[14] M.L. Kantam, T. Bandyopadhyay, A. Rahman, N.M. Reddy, B.M. Choudary, J. Mol. Catal. A Chem. 133 (1998) 293.
[15] B. Coq, A. Tijani, R. Dutartre, F. Figuéras, J. Mol. Catal. 79 (1993) 253.
[16] A. Tijani, B. Coq, F. Figuéras, Appl. Catal. 76 (1991) 255.
[17] X.-X. Han, R.-X. Zhou, G.-H. Lai, B.-H. Yue, X.-M. Zheng, J. Mol. Catal. A Chem. 209 (2004) 83.
[18] B. Coq, A. Tijani, F. Figuéras, J. Mol. Catal. 71 (1992) 317.
[19] Q. Xu, X.-M. Liu, J.-R. Chen, R.-X. Li, X.-J. Li, J. Mol. Catal. A Chem. 260 (2006) 299.
[20] G.C. Bond, D.T. Thompson, Cat. Rev. Sci. Eng. 41 (1999) 319.
[21] C. Mohr, H. Hofmeister, P. Claus, J. Catal. 213 (2003) 86.
[22] C. Milone, C. Crisafulli, R. Ingoglia, L. Schipilliti, S. Galvagno, Catal. Today 122 (2007) 341.
[23] E. Bus, J.T. Miller, J.A. van Bokhoven, J. Phys. Chem. B 109 (2005) 14581.
[24] R. Zanella, C. Louis, S. Giorgio, R. Touroude, J. Catal. 223 (2004) 328.
[25] P. Claus, A. Brückner, C. Mohr, H. Hofmeister, J. Am. Chem. Soc. 122 (2000) 11430.
[26] F. Cárdenas-Lizana, S. Gómez-Quero, N. Perret, M.A. Keane, Gold Bull., in press.
[27] M. Okumura, T. Akita, M. Haruta, Catal. Today 74 (2002) 265.
[28] R.J.H. Grisel, P.J. Kooyman, B.E. Nieuwenhuys, J. Catal. 191 (2000) 430.
[29] J.K. Nørskov, Rep. Prog. Phys. 53 (1990) 1253.
[30] A.C. Gluhoi, S.D. Lin, B.E. Nieuwenhuys, Catal. Today 90 (2004) 175.
[31] A.C. Gluhoi, M.A.P. Dekkers, B.E. Nieuwenhuys, J. Catal. 219 (2003) 197.
[32] M.O. Nutt, J.B. Hughes, M.S. Wong, Environ. Sci. Technol. 39 (2005) 1346.
[33] M.O. Nutt, K.N. Heck, P. Alvarez, M.S. Wong, Appl. Catal. B 69 (2006) 115.
[34] P. Sangeetha, P. Seetharamulu, K. Shanthi, S. Narayanan, K.S.R. Raob, J. Mol. Catal. A Chem. 273 (2007) 244.
[35] L.M. Sikhwivhilu, N.J. Coville, B.M. Pulimaddi, J. Venkatreddy, V. Vishwanathan, Catal. Commun. 8 (2007) 1999.
[36] V. Vishwanathan, V. Jayasri, P.M. Basha, N. Mahata, L.M. Sikhwivhilu, N.J. Coville, Catal. Commun. 9 (2008) 453.
[37] R. Zanella, S. Giorgio, C.R. Henry, C. Louis, J. Phys. Chem. B 106 (2002) 7634.
[38] G. Tavoularis, M.A. Keane, J. Chem. Technol. Biotechnol. 74 (1999) 60.
[39] G. Yuan, M.A. Keane, Chem. Eng. Sci. 58 (2003) 257.
[40] A. Sandoval, A. Gómez-Cortés, R. Zanella, G. Díaz, J.M. Saniger, J. Mol. Catal. A Chem. 278 (2007) 200.
[41] C. Baatz, U. Prüße, J. Catal. 249 (2007) 34.
[42] Y.-J. Chen, C.-T. Yeh, J. Catal. 200 (2001) 59.
[43] A.C. Gluhoi, X. Tang, P. Marginean, B.E. Nieuwenhuys, Top. Catal. 39 (2006) 101.
[44] C.K. Costello, J. Guzman, J.H. Yang, Y.M. Wang, M.C. Kung, B.C. Gates, H.H. Kung, J. Phys. Chem. B 108 (2004) 12529.
[45] E. Bus, R. Prins, J.A. van Bokhoven, Phys. Chem. Chem. Phys. 9 (2007) 3312.
[46] A. Hugon, L. Delannoy, C. Louis, Gold Bull. 41 (2008) 127.
[47] S.M. Oxford, J.D. Henao, J.H. Yang, M.C. Kung, H.H. Kung, Appl. Catal. A 339 (2008) 180.
[48] C.-H. Lin, S.D. Lin, J.-F. Lee, Catal. Lett. 89 (2003) 235.
[49] F. Arena, P. Famulari, N. Interdonato, G. Bonura, F. Frusteri, L. Spadaro, Catal. Today 116 (2006) 384.
[50] G.J. Hutchings, Catal. Today 100 (2005) 55.
[51] E.D. Park, J.S. Lee, J. Catal. 186 (1999) 1.
[52] A.P. Kozlova, A.I. Kozlov, S. Sugiyama, Y. Matsui, K. Asakura, Y. Iwasawa, J. Catal. 181 (1999) 37.
[53] V. Ferrer, A. Moronta, J. Sánchez, R. Solano, S. Bernal, D. Finol, Catal. Today 107–108 (2005) 487.
[54] F. Pinna, F. Menegazzo, M. Signoretto, P. Canton, G. Fagherazzi, N. Pernicone, Appl. Catal. A 219 (2001) 195.
[55] M. Hosseini, S. Siffert, H.L. Tidahy, R. Cousin, J.-F. Lamonier, A. Aboukais, A. Vantomme, B.-L. Su, Catal. Today 122 (2007) 391.
[56] P. Claus, Appl. Catal. A 291 (2005) 222.
[57] B. Hammer, J.K. Nørskov, Nature 376 (1995) 238.
[58] J. Harris, Surf. Sci. 221 (1989) 335.
[59] H.-S. Oh, J.H. Yang, C.K. Costello, Y.M. Wang, S.R. Bare, H.H. Kung, M.C. Kung, J. Catal. 210 (2002) 375.
[60] K. Hadjiivanov, G. Vayssilov, Adv. Catal. 47 (2002) 347.
[61] E.A. Sales, J. Jove, M.d.J. Mendes, F. Bozon-Verduraz, J. Catal. 195 (2000) 88.
[62] M.A. Bollinger, M.A. Vannice, Appl. Catal. B 8 (1996) 417.
[63] J.D. Grunwaldt, M. Maciejewski, O.S. Becker, P. Fabrizioli, A. Baiker, J. Catal. 186 (1999) 458.
[64] S. Minicò, S. Scirè, C. Crisafulli, A.M. Visco, S. Galvagno, Catal. Lett. 47 (1997) 273.
[65] F. Boccuzzi, A. Chiorino, M. Manzoli, D. Andreeva, T. Tabakova, J. Catal. 188 (1999) 176.
[66] J.Y. Lee, J. Schwank, J. Catal. 102 (1986) 207.
[67] M. Manzoli, A. Chiorino, F. Boccuzzi, Surf. Sci. 532 (2003) 377.
[68] F. Boccuzzi, A. Chiorino, S. Tsubota, M. Haruta, Catal. Lett. 29 (1994) 225.
[69] T. Diemant, Z. Zhao, H. Rauscher, J. Bansmann, R.J. Behm, Top. Catal. 44 (2007) 83.
[70] T.A. Baker, C.M. Friend, E. Kaxiras, J. Am. Chem. Soc. 130 (2008) 3720.
[71] I. Sobczak, A. Kusior, J. Grams, M. Ziolek, J. Catal. 245 (2007) 259.
[72] B. Qiao, Y. Deng, Appl. Catal. B 66 (2006) 241.
[73] J. France, P.J. Hollins, J. Electron Spectrosc. Relat. Phenom. 64 (1993) 251.
[74] J.-D. Grunwaldt, A. Baiker, J. Phys. Chem. B 103 (1999) 1002.
[75] T. Venkov, K. Fajerwerg, L. Delannoy, H. Klimev, K. Hadjiivanov, C. Louis, Appl. Catal. A 301 (2006) 106.
[76] F. Boccuzzi, A. Chiorino, M. Manzoli, Surf. Sci. 454–456 (2000) 942.
[77] Z.-X. Gao, Q. Sun, H.-Y. Chen, X. Wang, W.M.H. Sachtler, Catal. Lett. 72 (2001) 1.
[78] T. Wei, J. Wang, D.W. Goodman, J. Phys. Chem. C 111 (2007) 8781.
[79] K. Luo, T. Wei, C.-W. Yi, S. Axnanda, D.W. Goodman, J. Phys. Chem. B 109 (2005) 23517.
[80] C.W. Yi, K. Luo, T. Wei, D.W. Goodman, J. Phys. Chem. B 109 (2005) 18535.
[81] A.M. Venezia, V.L. Parola, G. Deganello, B. Pawelec, J.L.G. Fierro, J. Catal. 215 (2003) 317.
[82] S. Jujjuri, E. Ding, E.L. Hommel, S.G. Shore, M.A. Keane, J. Catal. 239 (2006) 486.
[83] H. Sakurai, M. Haruta, Appl. Catal. A 127 (1995) 93.
[84] C. Milone, R. Ingoglia, L. Schipilliti, C. Crisafulli, G. Neri, S. Galvagno, J. Catal. 236 (2005) 80.
[85] S. Schimpf, M. Lucas, C. Mohr, U. Rodemerck, A. Brückner, J. Radnick, H. Hofmeister, P. Claus, Catal. Today 72 (2002) 63.
[86] J.E. Bailie, H.A. Abdullah, J.A. Anderson, C.H. Rochester, N.V. Richardson, N. Hodge, J.G. Zhang, A. Burrows, C.J. Kiely, G.J. Hutchings, Phys. Chem. Chem. Phys. 3 (2001) 4113.
[87] J. Jia, K. Haraki, J.N. Kondo, K. Domen, K. Tamaru, J. Phys. Chem. B 104 (2000) 11153.
[88] L. Stobiński, L. Zommer, R. Duś, Appl. Surf. Sci. 141 (1999) 319.